Softening Kinetics in the Subcritical Heat-Affected Zone of Dual-Phase Steel Welds

E. BIRO, J.R. McDERMID, J.D. EMBURY, and Y. ZHOU

Welds in dual-phase (DP) steels exhibit heat-affected zone (HAZ) softening in which the tempered or subcritical HAZ exhibits a lower hardness *vs* that of the parent material. The rate of this softening reaction with respect to welding heat input was determined for four DP steels by making several bead-on-plate laser welds using a variety of heat inputs and measuring the resulting minimum hardness. The reduction in hardness was then fit to the Avrami equation, enabling a comparison of the relative heat needed to soften each steel. It was found that the heat input required for HAZ softening decreased as the C content of the martensite within the DP structure increased. However, the presence of carbide forming alloying elements such as Cr and Mo was able to increase resistance to softening.

DOI: 10.1007/s11661-010-0323-2

I. INTRODUCTION

WITH the implementation of legislation to increase automotive fuel efficiency,[1] automakers are seeking a variety of means to reduce vehicle weight. One of the ways that this is being accomplished is by replacing traditional steel grades with advanced high-strength steels (AHSS). This allows the steels to be downgauged, thereby reducing overall part weight.[2] Dual-phase (DP) steels are one of the commonly used AHSS grades being adopted by automakers.

DP steels derive their strength from a composite microstructure comprising ferrite, martensite, and bainite. However, as martensite is a thermally unstable phase, it will tend to decompose in the heat-affected zone (HAZ), resulting in softening of the local microstructure. This phenomenon has long been recognized and is typically known as HAZ softening.[3,4] HAZ softening is unavoidable in DP steels and occurs in the tempered or subcritical HAZ where the temperatures experienced during welding do not exceed the Ac_1 temperature of the material.[4,5] As martensite tempering fundamentally changes the DP microstructure, the mechanical properties of this area of the HAZ are characterized by a decrease in the yield and ultimate tensile strength, an increase in ductility, and the return of yield point elongation.[6] HAZ softening may also lead to strain localization and failure in the subcritical HAZ at stresses below the base material's ultimate tensile strength.[5,7]

As HAZ softening can have an adverse effect on weldment strength, much work has been done to characterize this phenomenon. It has been determined that HAZ softening is a very complex phenomenon and is affected by: microstructure martensite content, steel chemistry, heat input, and prestrain.[6–10] The potential hardness difference between the softened HAZ and the base material is proportional to the steel martensite content.[6,8] Steel alloy content can decrease HAZ softening by impeding the softening rate.[9] Increasing heat input (increasing the ratio of welding power to travel speed) increases HAZ softening as the local temperature of the subcritical HAZ is elevated for longer times, further advancing the tempering reaction.[7–10] Finally, prestrain has been seen to increase the overall magnitude of HAZ softening while increasing the absolute hardness of the softening region.[6,9]

Although considerable work has been done to characterize the effects of different material and processing parameters on HAZ softening, there has been no systematic study examining how the chemistry and microstructure of DP steels affect martensite tempering reaction kinetics occurring during the short time scales of welding. This study reports on how changing heat input affected HAZ softening in four DP steels: two DP600s and two DP780s. The resulting softening curves from welds in all four materials were then compared by normalizing the softening data, and the observed softening kinetics related to the steel metallurgy.

II. METHODOLOGY

A. *Materials*

Experiments were carried out on four industrially produced steels: two DP600 steels and two DP780 steels. These steels were chosen as their microstructures and

E. BIRO, Doctoral Student and Scientist, is with the Department of Materials Science and Engineering, McMaster University, L8S 4L8, and with ArcelorMittal Global Research, L8N 3J5, Hamilton, Ontario, Canada. J.R. McDERMID, Associate Professor, is with the Department of Mechanical Engineering, McMaster University. Contact e-mail: mcdermid@mcmaster.ca J.D. EMBURY, Professor Emeritus, is with the Department of Materials Science and Engineering, McMaster University. Y. ZHOU, Professor, is with the Department of Mechanical and Mechatronics Engineering, University of Waterloo, N2L 3G1, Waterloo, Ontario, Canada.

Manuscript submitted March 9, 2010.
Article published online June 10, 2010

chemistries were significantly different from each other, allowing a determination of how these factors affected softening kinetics. Both of the DP600s had relatively rich chemistries, being alloyed with higher amounts of carbide stabilizing elements, with one alloyed with Cr and the other alloyed with both Cr and Mo. The DP780s examined represent both rich and lean chemistry philosophies. The rich chemistry was alloyed with C, Mn, Si, Cr, and Mo, whereas the lean chemistry was only alloyed with C, Mn, and Si.

All materials were produced *via* the conventional industrial processing route of casting, hot rolling, and pickling followed by cold rolling. The two DP600 and rich DP780 materials were subsequently processed through a continuous galvanizing line in which the materials were intercritically annealed, rapidly cooled, and dipped in a conventional high Al galvanizing bath. The lean DP780 was processed in a similar manner (intercritical annealing and rapid cooling) through a continuous annealing line but was not coated with zinc.

Detailed characteristics of the as-received (base) steels may be found in Table I where the chemistries of the steels are listed in weight percent with the atomic percent of the alloying additions in parentheses. Table I also includes a summary of the microstructure of each base steel, where martensite volume percent and the sum of the martensite and bainite volume percent are listed as f_{mart} and f_{MA}, respectively. Due to C partitioning during the creation of the DP microstructure, the martensite and bainite C content was estimated separately from the steel bulk C content. This was calculated by assuming that the C content of the ferrite phase was 0.02 wt pct with the remaining C being partitioned equally between the martensite and bainite phases. Finally, the hardenability of the steels were compared using Yurioka's carbon equivalent equation (CE_N).[11] The microstructures of the as-received base materials are shown in Figure 1. It should be noted that limited autotempering was seen in the martensite phase of all of the steels examined (inset micrographs in Figure 1). This autotempering likely arose from the lower cooling rates after final thermal processing. However, significant volume fractions of untempered martensite were also present in the microstructures of the DP600 steels (Figures 1(a) and (b)).

B. *Welding*

All samples were laser welded in the bead-on-plate orientation. High heat input welds (welds made with higher power per unit length) were made using a 4-kW diode laser, and low heat input welds were made using an 8-kW CO_2 laser (operated at 80 pct power) in the case of the DP600s and a 1-kW Yb fiber laser in the case of the DP780s. The characteristics of all of the lasers may be found in Table II.

C. *Measuring Welding Heat Input*

Although three lasers were used to create the welds used in this study, the softening results for each experimental condition were compared on the basis of welding heat input. To avoid determining the influence of beam diameter, material absorptivity, and welder efficiency, heat input was calculated directly from the HAZ microstructure per the methodology of Xia *et al.*[8] This technique involves measuring the distance from the weld centerline to both the fusion boundary and to the edge of the intercritical zone where the peak temperatures reached during welding were the steel's melting point and Ac_1 temperatures, respectively (Figure 2). Using these measurements, the heat input could be calculated using Rosenthal's two-dimensional solution for weld zone temperature[8]:

$$\frac{Q_{\text{net}}}{vd} = \frac{\rho c_{\text{p}} (r_{\text{Ac}_1} - r_{\text{m}})(2\pi e)^{\frac{1}{2}}}{\left(\frac{1}{T_{\text{Ac}_1} - T_0} - \frac{1}{T_{\text{m}} - T_0}\right)} \quad [1]$$

where Q_{net} is the welding power, v the welding speed, d the plate thickness, ρ the material density, c_{p} the material specific heat capacity, and T_{Ac_1}, T_{m}, and T_0 are the Ac_1, melting, and ambient temperatures, respectively.

To impart a physical meaning to the heat input, it was converted into a time constant similar to that used by Ion *et al.*[12] In the present case, the time constant represents the time to heat a point in the weld HAZ from ambient temperature to its Ac_1 temperature. Thus, if a weld is made with a high heat input (slow welding speed), it will require significant time for the HAZ to reach the Ac_1 temperature, resulting in a large time

Table I. Details of Base Materials Used in Study. Steel Chemistries Given in Wt Pct (At. Pct)

Grade	DP600	DP600	DP780	DP780
Design	Cr	Cr/Mo	Rich Chemistry	Lean Chemistry
Thickness (mm)	2.0	2.0	2.0	1.5
C	0.10	0.11	0.15	0.10
Mn	1.8	1.6	1.9	1.8
Si	0.14 (0.29)	0.19 (0.38)	0.23 (0.45)	0.33 (0.64)
Cr	0.34 (0.36)	0.22 (0.23)	0.32 (0.35)	0.02 (0.02)
Mo	0.01 (0.00)	0.20 (0.12)	0.11 (0.06)	0.02 (0.01)
CE_N	0.35	0.36	0.52	0.31
f_{Mart} (pct)	2.9	3.5	9.3	17.0
f_{MA} (pct)	27.4	22.8	14.7	17.0
Base hardness (VHN)	194	214	243	249
Martensite C content (calculated wt pct)	0.31	0.41	0.90	0.49

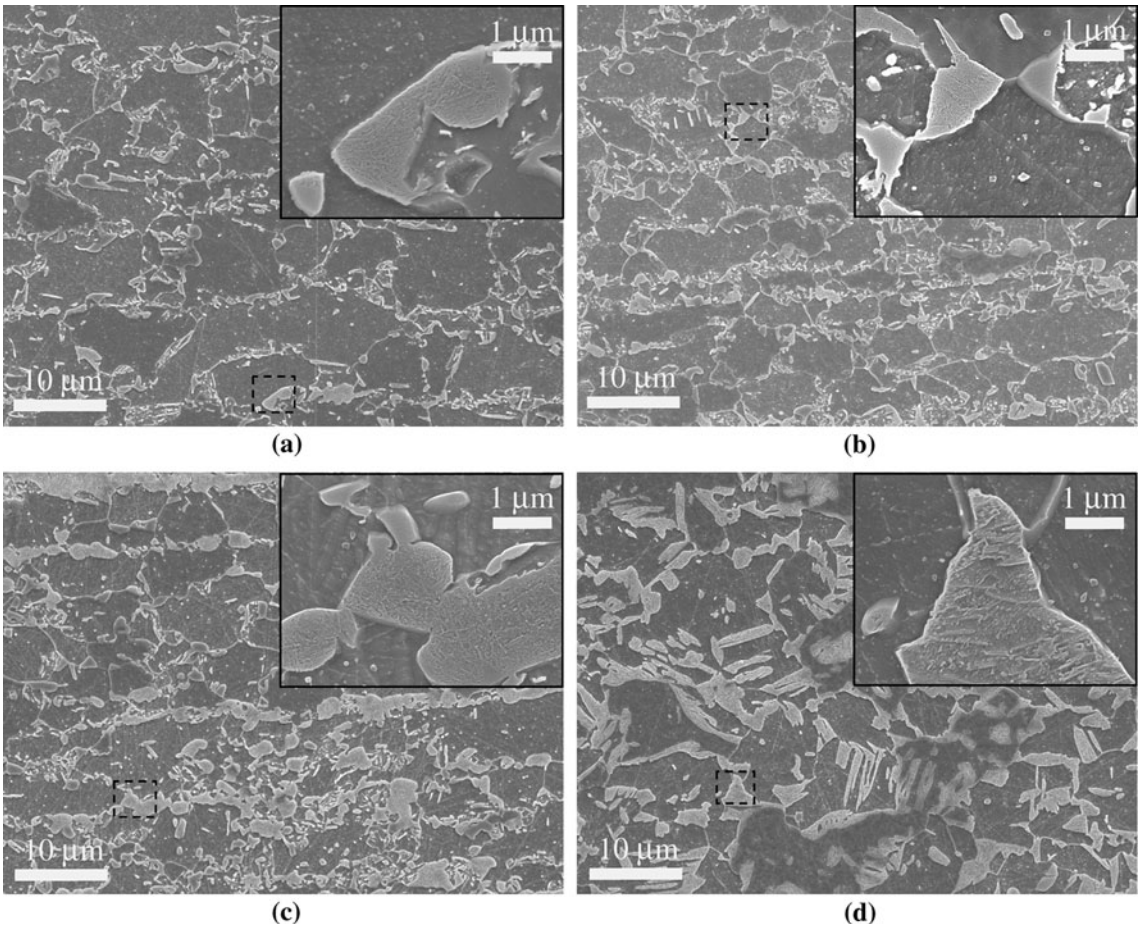

Fig. 1—Base material microstructures of (*a*) Cr DP600, (*b*) Cr/Mo DP600, (*c*) rich chemistry DP780, and (*d*) lean chemistry DP780. Increased magnification of autotempered martensite from indicated areas are shown in the micrograph insets.

Table II. Laser Characteristics Used for Welding

Laser Machine	Laser Source	Wave Length (μm)	Power (kW)	Beam Size (mm)
Nuvonyx ISL-4000	Diode	0.81	4.0	0.9 × 12
IPG Photonics—YLR-1000	Ytterbium Fiber	1.07	1.0	0.6
Trumpf TFL Turbo 8000	CO_2	10.6	6.4	0.6

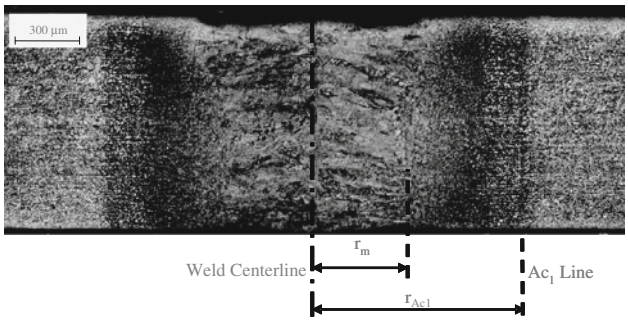

Fig. 2—Cross section of a typical weld showing the distance from the centerline to the fusion boundary (r_m) and the edge of the inter-critical zone (r_{Ac1}) (taken from Ref. 8).

constant, and the opposite is true if a weld is made with a low heat input. The time constant, as defined by Xia *et al.*,[8] is given by:

$$\tau = \frac{1}{4\pi e \lambda \rho c_p} \frac{[Q_{net}/(vd)]^2}{(T_{Ac_1} - T_0)^2} \quad [2]$$

where τ is the time constant and λ the thermal conductivity of the base material. Thus, weld heat input increases as the value of τ increases.

D. *Sample Preparation*

All samples for metallurgical analysis were similarly prepared. Transverse cross sections were cut from each

weld well away from both the weld start and crater. Samples were then hot-mounted and polished using standard metallographic techniques to a 1-μm diamond finish using an automatic polishing system (Struers RotoPol-31, Struers RotoForce-4, and a Struers Multidoser, Ballerup, Denmark).

E. *Microhardness*

Microhardness measurements were carried out on etched (2 pct nital) metallographic samples using a Vickers indenter with a 200-g load and a 15-second dwell time. All reported measurements are the average of three points measured in the through-thickness direction of the sample cross section, and base material measurements are an average of nine measurements. The error bars represent one standard deviation of the hardness readings. The trend lines presented are mathematical best fits.

F. *Electron Microscopy*

Scanning electron microscopy (SEM) was used to characterize the base material and identify the state of decomposition of the martensite within the HAZ after welding. The microstructure of the materials was revealed by etching the mounted and polished samples with 2 pct nital for 2 seconds. All SEM images were taken using a JEOL-7000F (Japan Electron Optics Ltd., Tokyo, Japan) field emission SEM with an acceleration voltage of 15 keV.

The decomposition products of the tempered martensite were imaged and identified from extraction replicas with a Philips CM-12 (Royal Philips Electronics, Amsterdam, The Netherlands) transmission electron microscope (TEM) using an acceleration voltage of 120 keV. Replicas were prepared by etching the cross-sectioned and polished samples with 2 pct nital for about 1 second to reveal the weld microstructure. After etching, all areas of the samples, with the exception of the subcritical HAZ, were masked with stop-off lacquer. The samples were then carbon coated using vapor deposition. After coating, the carbon film was cut and then lifted from the sample surface by immersing the sample in 5 pct nital. When the films floated from the sample surface, they were transferred to a dilute solution of methanol in water where they were picked up on a 200-mesh Cu TEM grid. All images were taken in bright-field mode. Select area diffraction (SAD) patterns were generated using a beam diameter of 700 nm and various camera lengths depending on the pattern. The camera constant may be found on each SAD pattern.

III. RESULTS

A. *Softening in DP Steels*

For all experimental welds, the minimum weldment hardness was found to be significantly less than the base material hardness (Figures 3 and 4). The minimum weldment hardness was a function of weld heat input where softening increased as the time constant (τ)

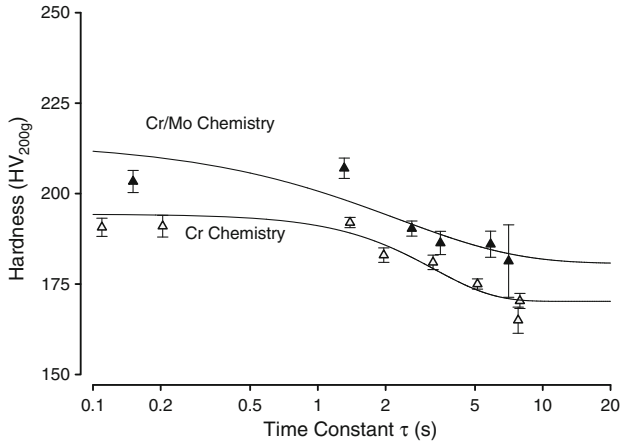

Fig. 3—Minimum HAZ hardness *vs* time constant for DP600 materials. Note that weld heat input increases with increasing τ, per Eq. [2].

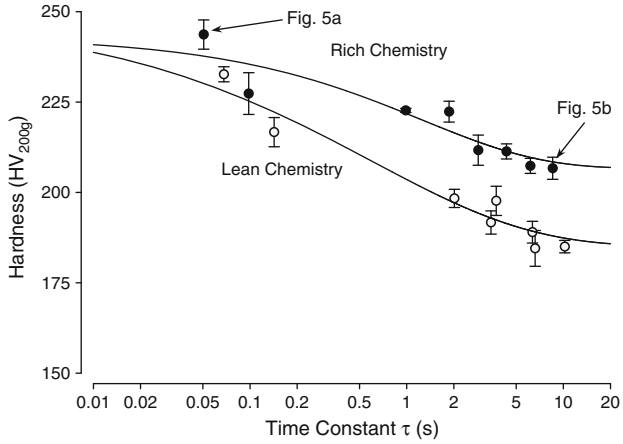

Fig. 4—Minimum HAZ hardness *vs* time constant for DP780 materials and the time constants of the welds examined in Fig. 5. Note that weld heat input increases with increasing τ.

increased (*i.e.*, higher heat input) until a minimum hardness was reached, which matches with past work.[8,9] However, when the hardness–time constant relation for each material pair were overlaid, it was difficult to compare the heat needed to soften the steels as either the initial or the final hardness observed for each material was different. This is to be expected, as all of the materials in this study had different martensite contents, which determines the maximum possible hardness drop.[8] However, if the rate of reduction in hardness for the materials is to be compared, then the curves must be normalized such that they represent the progress of the softening reaction rather than reduction in material hardness.

B. *Decomposition Products in Low and High Heat Input Welds*

Before a transformation may be applied to the hardness data, the martensite decomposition products formed in the HAZ of the welds as a function of weld

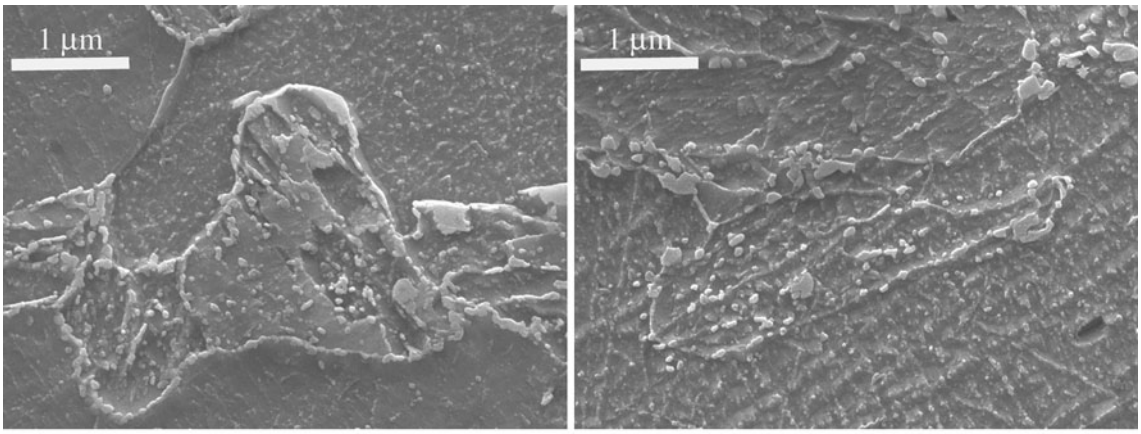

Fig. 5—Martensite phase found in the softened HAZ from (*a*) low and (*b*) high heat input welds from the lean DP780 steel.

heat input and alloy chemistry need to be characterized to determine if it was the same for all experimental conditions. Under SEM imaging, it was revealed that not all of the martensite decomposed immediately. After welding with low heat input, a patchwork of martensite decomposition was seen within some martensite grains (Figure 5(a)). When the heat input was sufficiently high, massive decomposition of the martensite throughout the microstructure was observed (Figure 5(b)).

TEM examination of the decomposition products using extraction replicas revealed that the particulate martensite decomposition products from all conditions were irregularly shaped (Figures 6 and 7). In general, the particles found in the HAZ of welds made with high heat input were significantly larger (*via* 95 pct confidence intervals of the image analysis results) than those found in the HAZ of welds made with low heat input. SAD patterns obtained from these particles revealed that the particulate decomposition products were cementite.[13] This matches results by Jung *et al.*,[14] who observed that during nonisothermal tempering of martensitic steels, although ε carbides formed at low temperature, only cementite remained after tempering near the Ac_1 temperature. From the TEM observations of the replicas on the two DP780s and Jung *et al.*'s[14] results, it is assumed that cementite and ferrite will be the only martensite decomposition products present in the subcritical HAZ of the DP600 welds after welding, as the latter steels were similar to the rich DP780 steel in alloying philosophy and similar to the lean DP780 in CE_N.

IV. DISCUSSION

A. *Comparison of Softening Kinetics*

The analysis of the softened HAZ revealed that the martensite within the base material structure decomposed to cementite and ferrite. Although it is possible that ε carbide formed during the initial stages of heating, they were not observed in the subcritical HAZ after welding. This is consistent with the work of Wang *et al.*[15] who modeled martensite decomposition and found that ε carbides grow and dissolve quickly and showed that cementite formation and growth may be modeled independently of ε carbide. Furthermore, it was seen in the present results that the martensite did not immediately decompose after the material reached the Ac_1 temperature. Instead, when the material was tempered for short times, the martensite partially decomposed, and this transformation progressed as the time that the weld was held at the tempering temperature (τ) increased. Finally, after the carbide particles formed, they grew with increasing tempering time until the martensite was fully decomposed. This pattern of local nucleation, growth, and saturation of a transformation product may be well described by the Avrami equation of transformation[16]:

$$\phi = 1 - \exp(-kt^n) \qquad [3]$$

where ϕ is the volume fraction of martensite that has been transformed, k is a fitting parameter representing the energy barrier to the tempering transformation, t is the tempering time (τ is used in this study), and n is a fitting parameter related to the rate of the transformation.

To describe martensite decomposition using the Avrami equation, a parameter ϕ was defined such that ϕ equals zero when the material is in its base state (*i.e.*, the as-received base materials, as described in Figure 1 and Table I) and is defined as being equal to one when the material has been fully tempered or is at its minimum hardness, as was done by Mittemeijer *et al.*[17] ϕ was calculated using the following equation:

$$\phi = \frac{H_{\text{Base}} - H}{H_{\text{Base}} - H_{\text{min}}} \qquad [4]$$

where H_{Base} is the hardness of the base metal, H_{min} is the minimum hardness value measured in the HAZ for a given material, and H is the sample hardness. The use of the ϕ parameter is based on the assumption that the material hardness is an average of the hardness of the individual phases weighted by their respective volume

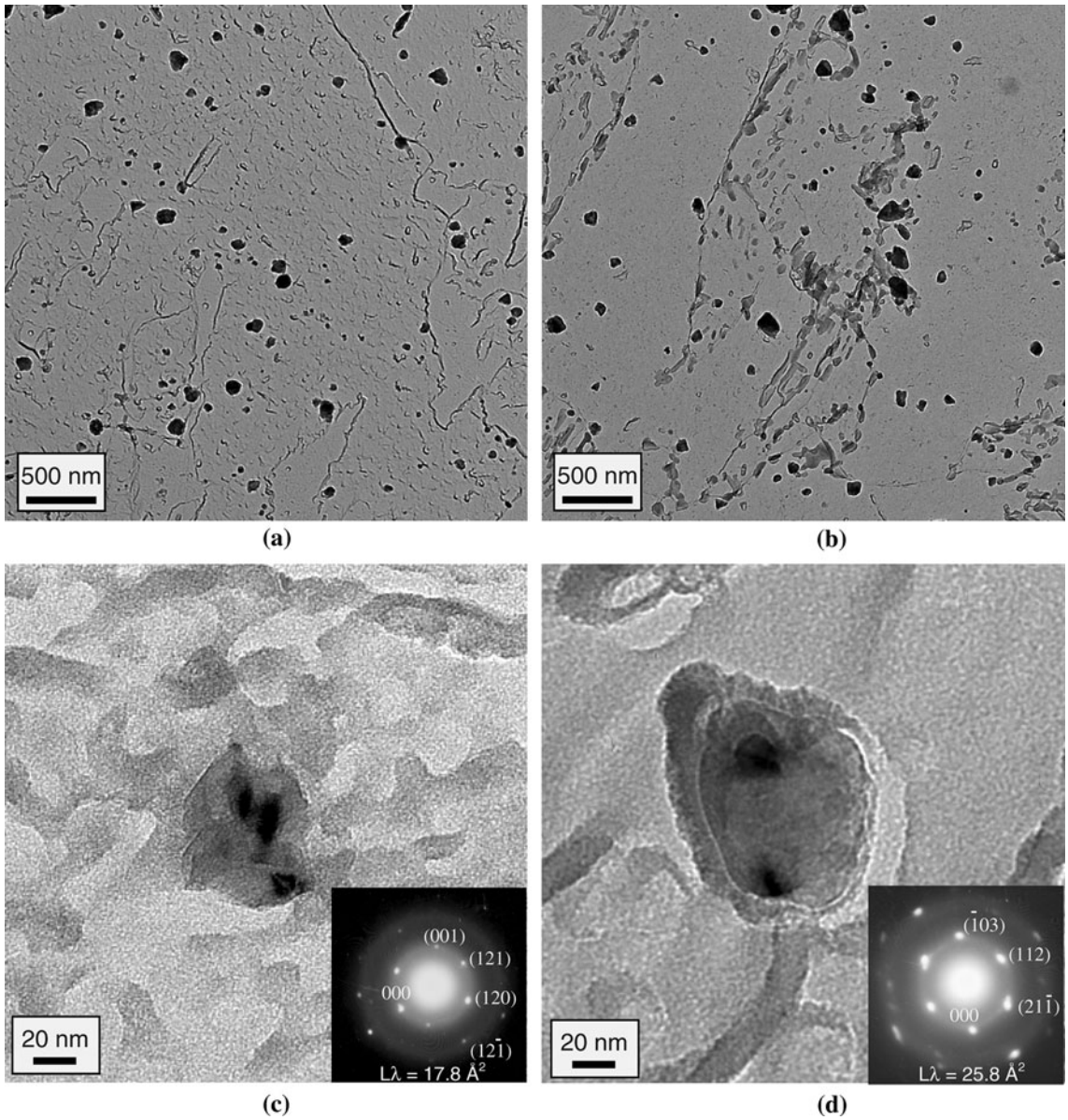

Fig. 6—TEM images of cementite particles found in the subcritical HAZ of the lean chemistry DP780 welded with (*a*) low and (*b*) high heat input as well as examples of individual particles and their SAD patterns from the welds made with (*c*) low and (*d*) high heat input.

percentages in the steel microstructure. Thus, the change in hardness observed in the subcritical HAZ is assumed to be due only to the changing volume percentages of the martensite, ferrite, and tempered martensite phases as the material tempers. However, it may also be possible that during tempering, the high internal stresses present in the DP steels are relieved. If this is the case, then changes in internal stresses will also be incorporated into the ϕ parameter. This must be confirmed with further work.

B. *Fitting Softening Kinetics to the Avrami Equation*

When all of the hardness data was transformed using Eq. [4], the softening kinetics of the DP600 and DP780 steels could be readily fit to the Avrami equation. The fits for all four steels were good, having adjusted r^2 values ranging between 0.81 and 0.92 (Table III). It is also interesting to note that the n parameter that was fit to the four materials was much lower than the range of 3 to 4 predicted by Avrami for pure particle nucleation and growth of a polyhedral particle.[16] However, it should be noted that the value of the n parameters for the DP780 materials were similar to those measured by Luppo and Ovejero-García[18] and Roberts *et al.*[19] who measured this parameter as 0.36 and 0.3, respectively. Roberts *et al.*[19] showed that if particle nucleation does not occur as Avrami described, but instead if the martensite phase decomposes as a receding front behind which the daughter products are formed (low carbon martensite and ε carbide in their case, and ferrite and cementite in the present case), then the n parameter

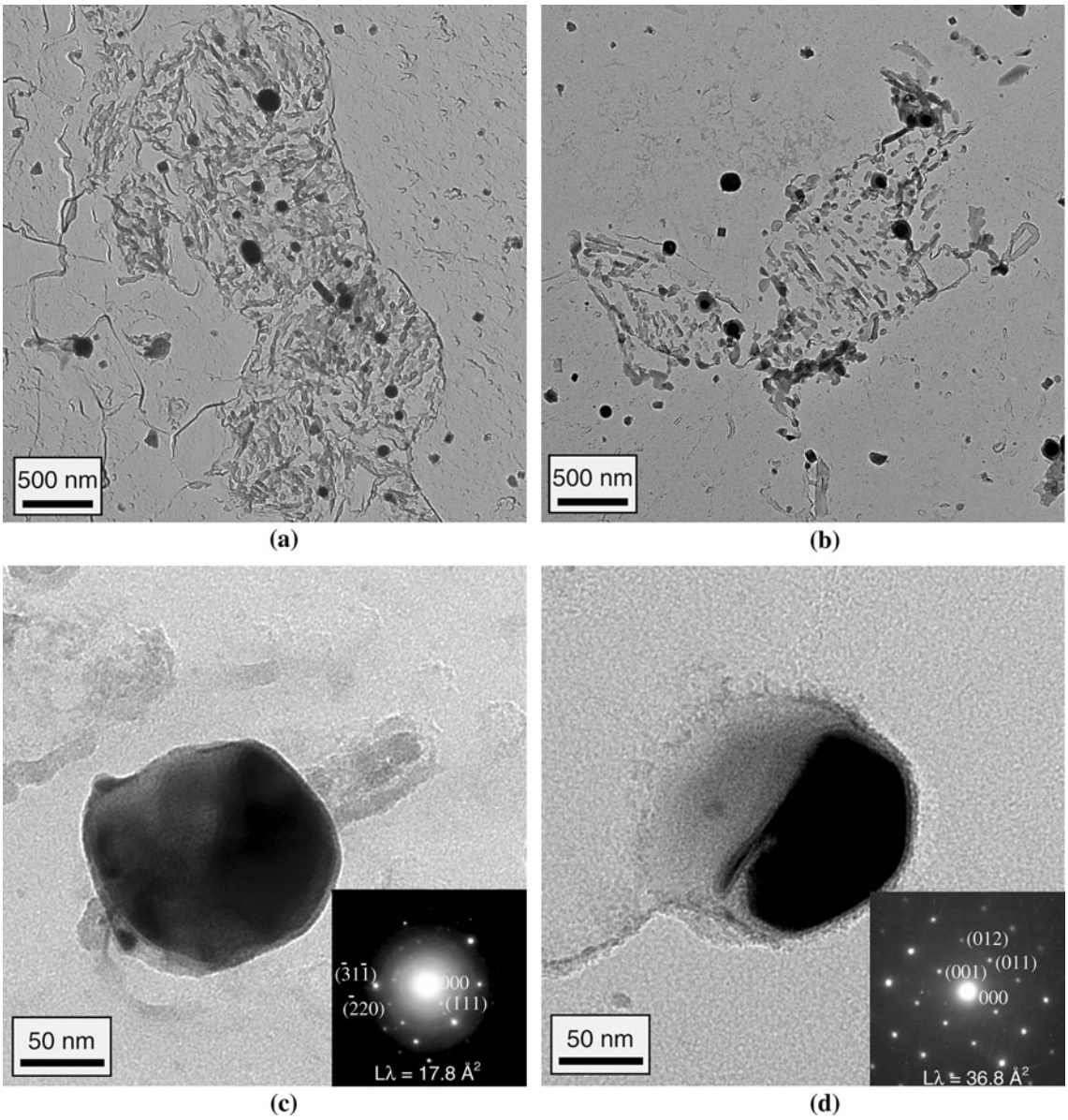

Fig. 7—TEM images of cementite particles found in the subcritical HAZ of the rich chemistry DP780 welded with (*a*) low and (*b*) high heat input as well as examples of individual particles and their SAD patterns from the welds made with (*c*) low and (*d*) high heat input.

Table III. Fitting Constants for the Avrami Equation

	DP600		DP780	
	Cr	Cr/Mo	Lean	Rich
k	0.14	0.20	1.23	0.91
n	1.60	1.73	0.42	0.58
Adjusted r^2	0.87	0.87	0.92	0.81

should be approximately 0.5, which matches the value measured for the DP780 steels. This appears to correlate with the observations in this study where martensite decomposed in a patchwork instead of at random and evenly distributed nucleation sites. However, in the case of the DP600 steels, where the n parameter was measured to be 1.6 and 1.7, it is possible that less of the martensite within these steels was autotempered, and there were nucleation sites available for the formation of cementite in the martensite within the as-received microstructure. So, cementite formed as a result of both the recession of the martensite front and nucleation created new cementite particles, resulting in an increase of the n parameter from that of the DP780 steels.

Now that the hardness data has been normalized with the ϕ parameter and fit to the Avrami equation, the progression of the tempering reactions for the four steels may be compared. It may be seen that the Cr/Mo DP600 softens at slightly shorter time constants than the Cr DP600, and the lean chemistry DP780 softens more rapidly than the rich chemistry DP780 (Figures 8 and 9). When the curves from both steel grades are overlaid,

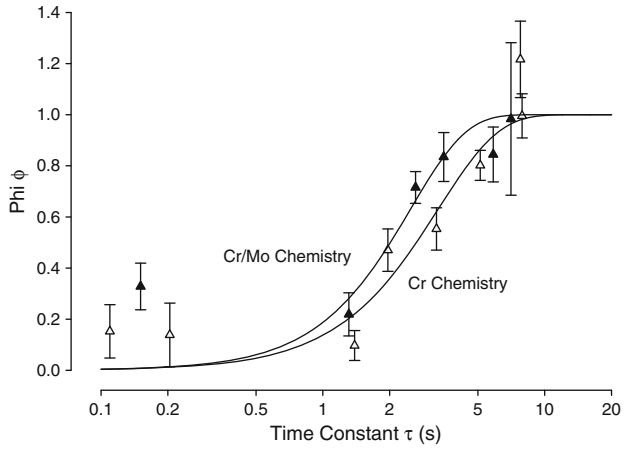

Fig. 8—Progression of martensite decomposition in DP600 steels as a function of weld time constant. Note that weld heat input increases with increasing τ.

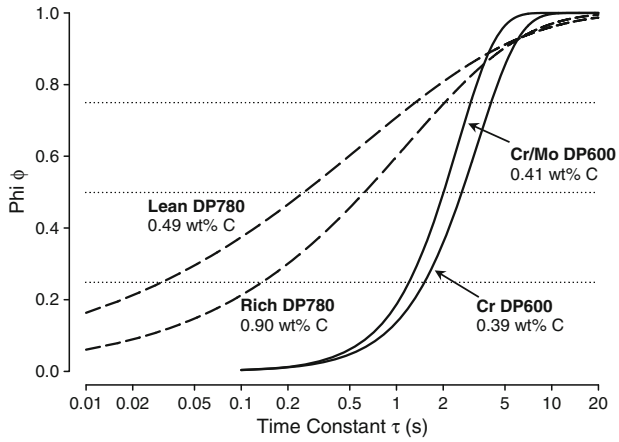

Fig. 10—Comparison of HAZ softening kinetics of all steels examined. The compositional information is the calculated martensite C content, per Table I.

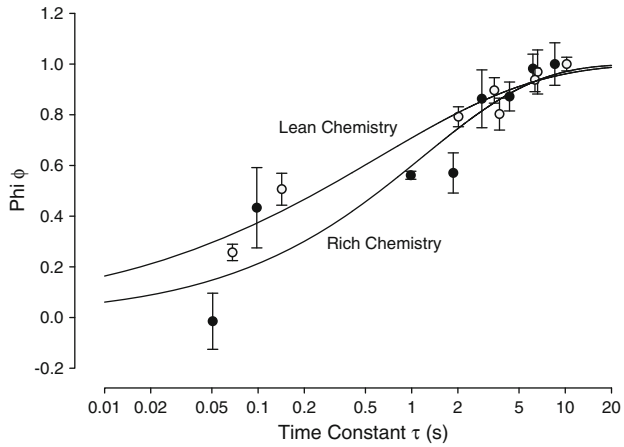

Fig. 9—Progression of martensite decomposition in DP780 steels as a function of weld time constant. Note that weld heat input increases with increasing τ.

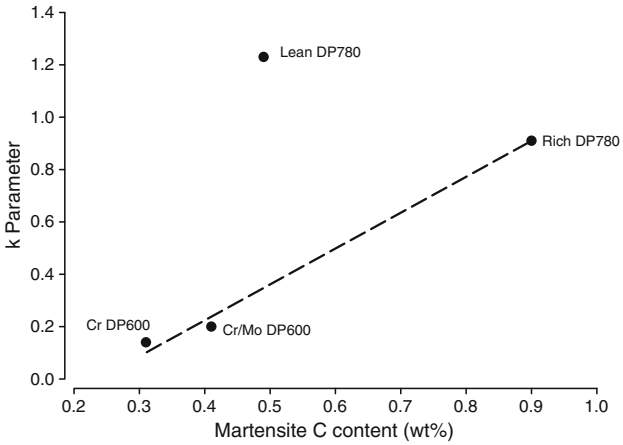

Fig. 11—Avrami k parameter *vs* martensite C content for all experimental steels.

general observations may be made on the softening kinetics as a function of overall steel chemistry (Figure 10). Although it has been suggested in the past that a high carbon equivalent indicates resistance to softening,[9] this was not observed in the present case. Figure 10 shows that the lean DP780 chemistry had the lowest resistance to softening, although its carbon equivalent was similar to the two DP600s (Table I), and the rich chemistry DP780 softened at a rate between that of the lean DP780 and the DP600s, despite its CE_N being the highest of the materials examined (Table I). However, with the exception of the lean DP780, the resistance to softening increased as the martensite C content decreased.

The effect of steel chemistry on the rate of martensite decomposition may be further illustrated using the k parameter from Avrami equation (Eq. [3]) where it can be seen that an increase in k results in a decrease in the time to initiate the tempering reaction. Thus, k can be thought of as representing the energy barrier to initiate HAZ softening, where higher values of k indicate a low-energy barrier and relatively easy initiation of HAZ softening and vice versa for lower values of k.

When the k parameters for the steels were compared, it was seen that k was proportional to the martensite C content for the three steels alloyed with carbide forming elements, with the lean DP780 k value being considerably above this curve (Figure 11). This disagrees somewhat with the results of Roberts *et al.*,[19] who showed that k is only a function of martensite C content. However, in that study, none of the steels were alloyed with carbide forming elements. In the present case, Figure 11 indicates that martensite decomposition is a function of both martensite C content and alloying chemistry; unfortunately, as only one steel was alloyed without Cr and Mo, we cannot know the relationship between k and martensite C content for this steel family without testing more materials.

It is logical that martensite C content controls the rate of the tempering reaction, as tempering is a diffusion-driven process where the C within the martensite diffuses into the surrounding material. As the martensite C content increases, the driving force for this reaction increases, speeding the tempering transformation. It is thought that the lean chemistry DP780 does not fit this model because it was alloyed without strong carbide formers such as Mo and Cr. These additions stabilize the martensite,[20] retarding the tempering reaction and resulting in the lean DP780 tempering with much lower welding heat when compared to materials with similar martensite carbon content.

V. CONCLUSIONS

Bead-on-plate welds were made on two DP600 and two DP780 steels with different chemistries. After welding, the hardness of the subcritical zone was measured and the following can be concluded about the HAZ softening observed:

1. The minimum HAZ hardness for all of the steels decreased as heat input increased until a minimum value was observed. Further increases in heat input had no further effect on subcritical HAZ hardness.
2. The martensite decomposition product in the subcritical HAZ for all welds was cementite.
3. Because HAZ softening by martensite tempering is a function of cementite nucleation, growth, and saturation, HAZ softening kinetics could be fit to the Avrami equation.
4. The heat required for HAZ softening decreased as the martensite C content increased in steels with similar amounts of carbide forming alloying additions (*i.e.*, Cr and Mo). This is consistent with a diffusion mechanism driving martensite decomposition.
5. The lean DP780 alloyed without Cr and Mo softened with a lower heat input than its martensite C content would suggest when compared to the other steels. This was attributed to its lack of carbide forming alloying elements that stabilized the martensite, thereby slowing the tempering reaction.

ACKNOWLEDGMENTS

The authors would like that the staff of the Canadian Centre for Electron Microscopy and Dr. X. Wang, who assisted with the preparation and the analysis of the TEM images and SAD patterns. The authors also wish to thank ArcelorMittal for providing the experimental materials used and for permission to publish this work.

REFERENCES

1. *Federal Register*, 2009, vol. 74, pp. 49454–789.
2. W. Gan, S.S. Babu, N. Kapustaka, and R.H. Wagoner: *Metall. Mater. Trans A*, 2006, vol. 37A, pp. 3221–31.
3. S. Hashimoto, S. Kanbe, and M. Sudo: *Trans. ISIJ*, 1981, vol. 21, p. B-497.
4. N. Yamauchi, T. Taka, K. Kunishige, and N. Nagao: *Trans. ISIJ*, 1982, vol. 22, p. B-107.
5. T. Taka, K. Kunishige, N. Yamauchi, and N. Nagao: *ISIJ Int.*, 1989, vol. 29, pp. 503–10.
6. E. Biro and A. Lee: *Sheet Metal Welding Conference XII*, AWS, Livonia, MI, 2006.
7. P.K. Ghosh, P.C. Gupta, Ramavtar, and B.K. Jha: *Weld. J.*, 1991, vol. 70, pp. 7s–14s.
8. M. Xia, E. Biro, Z. Tian, and Y.N. Zhou: *ISIJ Int.*, 2008, vol. 48, pp. 809–14.
9. E. Biro and A. Lee: *Sheet Metal Welding Conference XI*, AWS, Sterling Heights, MI, 2006.
10. P.K. Ghosh, P.C. Gupta, O.M. Pal, R. Avtar, B.K. Jha, and V.S. Dwivedi: *ISIJ Int.*, 1993, vol. 33, pp. 807–15.
11. N. Yurioka, H. Suzuki, S. Ohshita, and S. Saito: *Weld. J.*, 1983, vol. 62, pp. 147s–53s.
12. J.C. Ion, K.E. Easterling, and M.F. Ashby: *Acta Metall.*, 1984, vol. 32, pp. 1949–62.
13. K.W. Andrews, D.J. Dyson, and S.R. Keown: *Interpretation of Electron Diffraction Patterns*, 2nd ed., Plenum Press, New York, NY, 1971, pp. 181–91.
14. M. Jung, S-J Lee, and Y-K Lee: *Metall. Mater. Trans. A.*, 2009, vol. 40A, pp. 551–59.
15. Y. Wang, S. Denis, B. Appolaire, and P. Archambault: *J. Phys. IV France*, 2004, vol. 120, pp. 103–10.
16. J.W. Christian: *The Theory of Transformations in Metals and Alloys, Part I, Equilibrium and General Kinetic Theory*, 2nd ed., Pergamon Press, Oxford, UK, 1975, pp. 19–20.
17. E.J. Mittemeijer, A. Van Gent, and P.J. Van der Schaaf: *Metall. Trans. A*, 1986, vol. 17A, pp. 1441–45.
18. M.I. Luppo and J. Overjero-García: *Mater. Charact.*, 1998, vol. 40, pp. 189–96.
19. C.S. Roberts, B.L. Averbach, and M. Cohen: *Trans. AIME*, 1953, vol. 45, pp. 576–603.
20. E.C. Bain: *Alloying Elements in Steel*, 1st ed., ASM, Cleveland, OH, 1939, pp. 146–260.